Fast Three Dimensional Magnetic Resonance Imaging

Pablo Irarrazabal, Dwight G. Nishimura

To reduce the scan time in three-dimensional (3D) imaging, the authors consider alternative trajectories for traversing *k*-space. They differ from traditional 3D trajectories, such as 3DFT, in that they employ time-varying gradients allowing longer readouts and in turn a reduced scan time. Some of these trajectories reduce by an order of magnitude the number of excitations compared with 3DFT and provide flexibility for trading off signal-to-noise ratio for scan time. Other concerns are the minimum echo time and flow/motion properties. As examples, the authors show two applications: A 3D data set of the head (field of view of 30 × 30 × 7.5 cm and resolution of 1.5 × 1.5 × 1.5 mm) acquired in 56 s using a stack of spirals in 3D *k*-space; and a 3D movie of the heart (20 × 20 × 20 cm field of view, 2 × 2 × 2 mm resolution, and 16 time frames per cardiac cycle) acquired in 11 min using a cones trajectory.

Key words: MRI; fast imaging; 3D imaging; *k*-space trajectories.

INTRODUCTION

Besides minor considerations such as storage capacity and processing time, a primary consideration of 3D imaging techniques is their long scan time caused by the increased number of excitation necessary to acquire the data.

A 3D data set can be formed either by stacking slices (multi-slice acquisition) or by acquiring the data in the 3D Fourier domain. Compared with a multi-slice acquisition, a volumetric imaging sequence (intrinsically three-dimensional) has the following advantages: the image does not suffer from gaps or "crosstalk" between different slices (1, 2); isotropic resolution is easier to achieve (2); and the method is more flexible in providing a trade-off between SNR and scan time (3).

This paper demonstrate that alternative trajectories for sampling 3D *k*-space can be employed to shorten the scan time. Motivated by the successful use of spiral trajectories for 2D fast imaging (4), we employ volumetric imaging with time-varying gradients (5, 6). Although our goal is to traverse 3D *k*-space as fast as possible, we also consider insensitivity to flow and motion artifacts.

The new trajectories presented here allow faster coverage of *k*-space and therefore reduce the scan time. This feature makes current 3D applications faster, and also makes 3D imaging available for new applications.

MRM 33:656–662 (1995)

From the Information Systems Laboratory, Department of Electrical Engineering, Stanford University, Stanford, California.

Address correspondence to: Dwight G. Nishimura, Ph.D., Durand 302, Stanford, CA 94305.

Received August 24, 1994; revised December 9, 1994; accepted January 5, 1995.

This work was supported by NSF BCS 9058556, NIH HL 39297, NIH NS 29434, and GE Medical Systems.

P.I. is on leave from the Department of Electrical Engineering, Universidad Católica de Chile.

0740-3194/95 $3.00

THEORY

In the design of the new *k*-space trajectories presented in this paper, we consider the following issues.

The trajectories were designed to shorten the scan time by reducing the number of excitations. They differ from traditional 3D trajectories in that they employ time-varying gradients, so the sampling does not occur in a single straight line. Curved and echo-planar trajectories in general allow longer readouts and in turn reduce the scan time. These trajectories provide flexibility for trading off SNR for scan time. If SNR is important, it can always be recovered by averaging.

To achieve efficient acquisitions, it is required from the trajectories to sample *k*-space in the most uniform way possible. The design is restricted by hardware limitations: maximum gradient amplitude (speed along the trajectory) and maximum slew rate of the gradients (vectorial acceleration of the trajectory). The reconstruction procedure does not impose any further restriction. The data can be sampled in any fashion provided sufficient *k*-space, in the Nyquist sense, is acquired, that is, it is not possible to place a sphere of diameter 1/field-of-view in *k*-space without including at least one sample.

To obtain isotropic resolution, or equivalently, a spherically symmetric impulse response, a sphere in *k*-space needs to be sampled (7). In three dimensions, the time saving for sampling a sphere instead of a cube is 47.6%, compared with 21.5% for sampling a circle instead of a square in 2D. The same is true for ellipsoids with respect to parallelepipeds. Whenever possible we used this idea to reduce scan time.

An auxiliary goal is for the trajectories to achieve a certain level of insensitivity to flow and motion artifacts, which is especially important for cardiovascular applications. The motion/flow properties of the trajectories are compared on the basis of the two criteria proposed by Nishimura *et al.* (8) in their *k*-space formalism. To have good flow properties, the gradient's first moment should be small near the origin of *k*-space and smoothly varying as a function of *k*-space position.

Off-resonance effects are manifested as blurring for trajectories with spiral-like readouts (4) and were not considered in the design, although we avoided long readouts to reduce the phase accrual.

Trajectory Alternatives

We compared several *k*-space trajectories whose characteristics are summarized in Table 1.

For the sake of comparison, all the trajectories were designed with the following parameters: a field of view of 20 × 20 × 20 cm; a resolution of 100 × 100 × 100 pixels

Table 1
3D Trajectory Comparison

Trajectory	Total # of excitations	Scan time[a] (min:sec)	Prep. time[b] (ms)	Min. *TE*[c] (ms)
3DFT	10000	8:20	1.43	2.29
Cylindrical 3DFT	7854	6:33	1.43	2.29
3D echo planar	1667	1:23	1.43	2.29
Cylindrical 3D echo planar	1310	1:05	1.43	2.29
Stack of spirals	900	0:45	1.42	0
Shells	629	0:31	1.42	0
Spherical stack of spirals	628	0:31	1.42	0
3D PR	31416	26:10	0	0
Spiral-PR hybrid	1413	1:10	0	0
Cones	1152	0:57	0	0
Yarn	1044	0:52	0	0
Density compensated cones	800	0:40	0	0

The trajectories are presented in order of decreasing number of excitations, first for trajectories with a preparation time, then for trajectories without preparation time.
[a] Scan time is computed for a TR = 50 ms and each acquisition is 14.336 ms long.
[b] Preparation time is the maximum of the times required to go from the origin of k-space to the start of the acquisition.
[c] Minimum TE is the minimum time at which the origin of k-space is read.

or 2 × 2 × 2 mm; a readout duration of 14.336 ms; and a repetition time of TR = 50 ms. All trajectories are supported with the hardware constraints of

$$\text{Max}|\vec{G}| \leq 1 \text{ G/cm}$$

$$\text{Max}\left|\frac{d\vec{G}}{dt}\right| \leq 2 \text{ G/cm/ms}.$$

We first present four trajectories in which the sampling occurs on a Cartesian grid: Traditional 3DFT, 3D echo planar and a modified version of each that acquires a cylinder instead of a cube. For these trajectories the reconstruction is only a fast Fourier transform (FFT). Seven other trajectories are presented in which k-space is sampled nonuniformly. To obtain the sample values on a Cartesian grid, suitable for the FFT, a gridding algorithm (9) is employed. We describe the 3D gridding algorithm in detail in the next section. These trajectories include a stack of spiral, as proposed by Meyer *et al.* (10) and our proposed modification, a spherical stack of spiral; the shells that uses the same trajectory employed by Wong and Roos (11) for 3D excitation; a conventional 3D projection-reconstruction; and our three new trajectories: spiral-PR hybrid, yarn, and cones.

1. 3DFT (Fig. 1) A conventional 3DFT trajectory serves as reference. After each excitation, a constant gradient is applied such that a straight line is acquired in one k-space dimension. The advantages of this trajectory are its simplicity, ease of reconstruction, and short readouts. It uses less than the 14.336 ms specified with the design parameters, or conversely it has better SNR if the whole 14.336 ms are employed. The main disadvantage is its long scan time, as it requires 10,000 excitations (8 min 20 s). It also requires a preparation time of 1.43 ms and a minimum TE of 2.29 ms, as constrained by the time required to backup in the readout direction and/or to phase encode each acquisition. The 3DFT trajectory is sensitive to flow and motion artifacts. The magnitude of the gradient's first moment is significant near the origin of k-space. Flow compensation reduces the sensitivity at the expense of increasing the echo time. In any case, pulsatile motion produces artifacts due to phase discontinuities from readout to readout (12).

2. Cylindrical 3DFT (Fig. 2) The simplest modification to the 3DFT trajectory is to make the resolution more isotropic by restricting the k-space coverage to a cylinder. This trajectory has the same advantages as the regular 3DFT, but the number of required excitations is reduced to 7854 (6 min 33 s). It still has the same minimum TE requirement and sensitivity to flow artifacts.

3. 3D Echo Planar (Fig. 3) If more than one line in k-space is acquired in each readout, the number of excitations is reduced. This can be done by extending the idea of echo planar to three dimensions (13, 14). It requires 1667 excitations (1 min 23 s). It has the advantage of being easy to reconstruct and the disadvantage of not having good flow properties due to the phase encoding steps. The

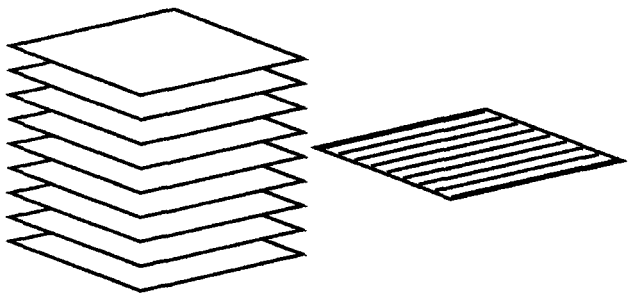

FIG. 1. 3DFT trajectory.

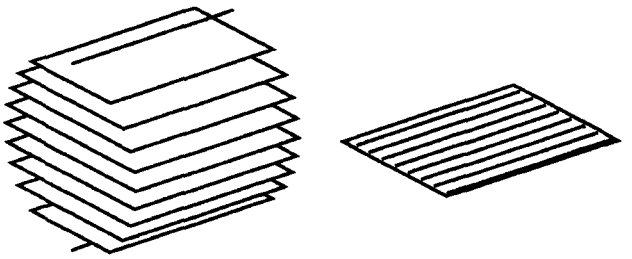

FIG. 2. Cylindrical 3DFT trajectory.

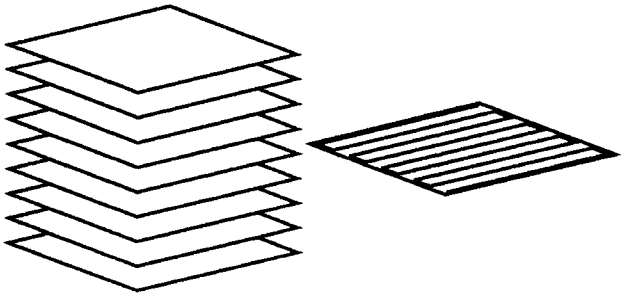

FIG. 3. 3D echo planar trajectory.

sequence has a preparation time of 1.43 ms and a minimum *TE* of 2.29 ms.

4. Cylindrical 3D Echo Planar (Fig. 4) As with the 3DFT trajectory the 3D echo planar trajectory can also be modified such that only a cylinder in *k*-space is acquired. This trajectory has the same advantages as the regular 3D echo planar, but the number of required excitations is reduced to 1310 (1 min 5 s). The minimum *TE* requirement and flow properties remain the same.

5. Stack of Spirals (Fig. 5) To reduce the number of excitations, a time-varying gradient trajectory based on spirals is considered. The stack of spirals is formed by placing one planar spiral acquisition on top of each other in *k*-space (10). The main advantage of this trajectory is that it reduces the number of excitations to 900 (45 s). Although the flow properties are relatively good in-plane (4, 8), there is still a phase encoding in the third dimension that produces ghosting artifacts under oscillatory motion and gives a preparation time of 1.42 ms. Since the sampling is not on a Cartesian grid, the reconstruction is more computationally intensive. A 2D gridding algorithm is employed for each plane in *k*-space.

6. Spherical Stack of Spirals (Fig. 6) By reducing the circle diameter and the number of interleaves of planes farther away from the origin, the stack of spiral is modified such that only a sphere is acquired. It has the same advantages and disadvantages as the stack of spirals, but reduces the number of excitations to 628 (31 s).

7. Shells (Fig. 7) Instead of acquiring planes in *k*-space, it is also possible to acquire spherical surfaces (11). After a phase encoding step that moves the *k*-space location from the origin to the pole of one of the concentric spheres, the trajectory spirals down on the surface of the sphere. As with the spherical stack of spirals this trajectory needs a phase encoding step that requires a preparation time of 1.42 ms and increases the sensitivity to pulsatile flow artifacts in one direction. In the other directions it possesses good flow properties. The advantage of this trajectory is its reduced number of excitations, 629 (31 s).

8. 3D Projection-Reconstruction (PR) (Fig. 8) A conventional trajectory for 3D *k*-space that does not have a minimum *TE* requirement is the 3D PR. The acquisition starts at the origin of *k*-space and moves along a straight line outwards. This trajectory is simple to implement and the readouts may be very short. It does not have a minimum *TE* requirement (the origin of *k*-space is acquired

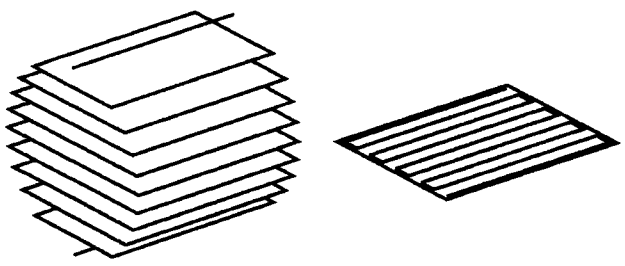

FIG. 4. Cylindrical 3D echo planar trajectory.

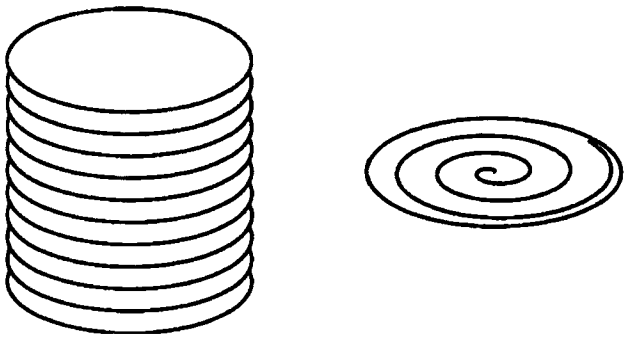

FIG. 5. Stack of spiral trajectory.

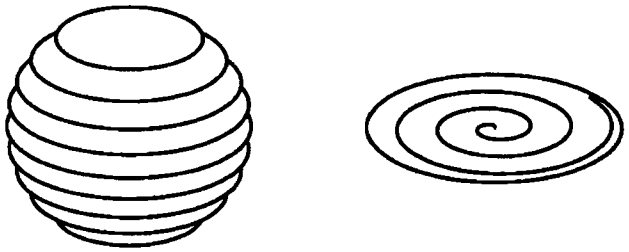

FIG. 6. Spherical stack of spiral trajectory.

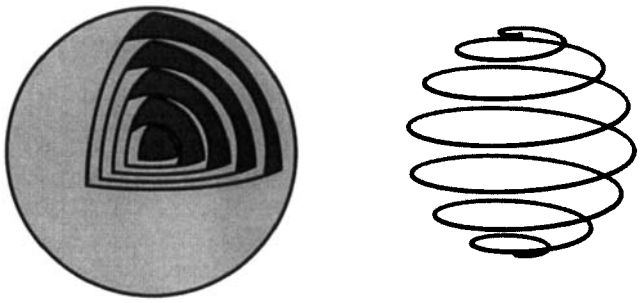

FIG. 7. Shells trajectory.

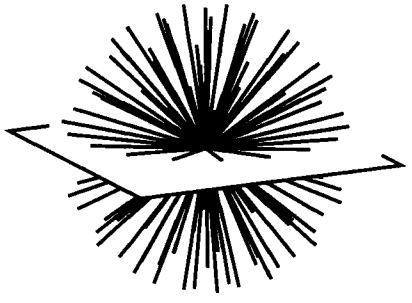

FIG. 8. 3D projection-reconstruction trajectory.

immediately after the excitation) and its flow properties are excellent (15, 16). The big disadvantage of this trajectory is, of course, a long total scan duration because it requires 31,416 excitations (26 min 10 s).

9. Spiral-PR Hybrid (Fig. 9) A trajectory that also avoids the minimum *TE* and the phase encoding step is the spiral-PR hybrid. Planar spiral trajectories are rotated around a common axis in their planes. This trajectory possesses all the advantages of a planar spiral—good flow properties and allows the trade off of scan time for SNR—and in addition it does not have a minimum *TE* requirement nor does it require phase encoding steps. As compared with the spherical stack of spiral, the price paid for these better properties is an increase in the number of excitations to 1413 (1 min 10 s).

10. Yarn (Fig. 10) The yarn trajectory is inspired by the way yarn is rolled into a ball. The natural tendency of rolling the yarn with the least possible curvature suits the hardware constraint of slew rate. It is defined as follows: Concentric circles are drawn on a plane (the radii differences are given by the desired field of view). The circles are divided into an integer multiple of the number of interleaves. Starting from the center, semi-circles perpendicular to the plane are drawn connecting opposite (as opposite as possible) points in the circles. Because this trajectory can be made with arbitrary readout lengths, it allows a trade-off between SNR and scan time. The minimum *TE* is zero and it has good flow properties. The yarn trajectory requires 1044 excitations (52 s). This trajectory is not simple to implement and care is required to make the sampling of *k*-space as uniform as possible.

11. Cones (Fig. 11) Another alternative is to use the cones trajectory. The surface of each concentric cone is traversed with a spiral-like trajectory. It requires 1152 excitations (57 s). It has good flow properties and the minimum *TE* is zero. As with all nonplanar and nonuniform trajectories, it requires a 3D gridding reconstruction algorithm. There is inefficiency in sampling *k*-space since there is oversampling near the origin.

A variant of this trajectory, the density compensated cones, reduces the oversampling by varying the pitch of the spiral as it gets farther away from the origin to compensate for the nonuniform separation between cones. It requires 800 excitations (40 s) and possesses all the advantages of the cones trajectory.

Reconstruction

To use the fast Fourier transform algorithm to reconstruct the data, it is necessary to map the nonuniformly sampled points to a Cartesian grid. This is done with a "gridding" algorithm described in this section.

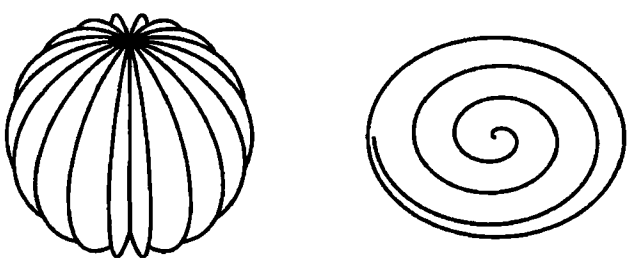

FIG. 9. Spiral-PR hybrid trajectory.

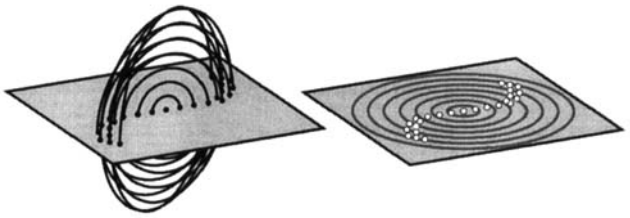

FIG. 10. Yarn trajectory.

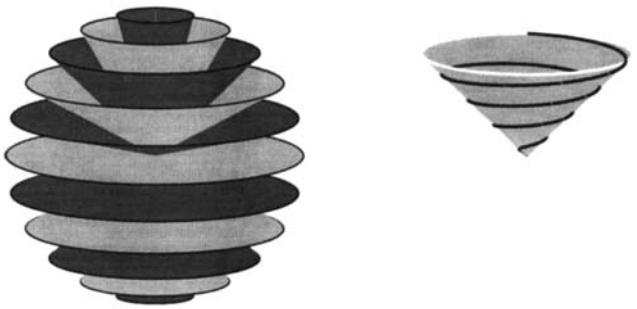

FIG. 11. Cones trajectory.

The idea of gridding (9, 17, 18) is to convolve the sampled data (M_s) with a kernel such that it is possible to obtain the value of the smoothed data at the grid points (M_c). The smoothing operation in the frequency domain can be undone with a division in the object domain, after the FFT operation.

The reconstruction is summarized as follows (subsequent paragraphs will analyze this in detail):

$$M_c(\mathbf{k}) = \left[\frac{M_s(\mathbf{k})}{\rho(\mathbf{k})} * C(\mathbf{k})\right] \cdot \mathrm{III}(\mathbf{k}) \qquad [1]$$

$$m_c(\mathbf{x}) = \frac{1}{c(\mathbf{x})}\mathbf{FT}_{3D}^{-1}(M_c(\mathbf{k})) \qquad [2]$$

The vector $\mathbf{x}$ describes the position in object-domain, $\mathbf{k}$ is the spatial-frequency vector, and $M_s(\mathbf{k})$ is the sampled data, defined by

$$M_s(\mathbf{k}) = M(\mathbf{k}) \cdot S(\mathbf{k}) \qquad [3]$$

where $S(\mathbf{k})$ is a set of delta functions located at the actual sampling points, defined by the *k*-space trajectory, and $M(\mathbf{k})$ is the continuous Fourier transform of the object $m(\mathbf{x})$.

M_s is divided by $\rho(\mathbf{k})$, the density of sampling in *k*-space, to compensate for the nonuniform weighting of M_s as a function of the position in *k*-space. The density of sampling can be computed as $\rho(\mathbf{k}) = S(\mathbf{k}) \cdot D(\mathbf{k})$, with $D(\mathbf{k})$ a convolving kernel which could be identical to $C(\mathbf{k})$ (17), or from an analytical expression such as the one used by Meyer *et al.* (4) for spirals. The density-compensated data is then convolved with a convolution kernel $C(\mathbf{k})$. The selection of C involves a trade-off between computational efficiency and aliasing in the resultant image (17). Our convolving kernel C is a separable triangular function with widths of $w_x = w_y = w_z = 1.45$

discrete k-space unit-values. It does not introduce any noticeable aliasing and is fast to compute.

$$C(\mathbf{k}) = \wedge(k_x/w_x) \wedge (k_y/w_y) \wedge (k_z/w_z) \quad [4]$$

$$\wedge(x) = \begin{cases} 1 - |x| \text{ if } |x| < 1 \\ 0 \text{ otherwise} \end{cases}$$

Finally, in Eq. [1], the convolved data is sampled onto a uniform grid. This is represented by a multiplication by III($\mathbf{k}$), a set of delta functions located at the grid points.

Equation [2] shows that the reconstructed image is not just the inverse Fourier transform of M_c. The effect of the convolution in the frequency domain, which is a multiplication in the object domain, must be undone by dividing the inverse transform of M_c by the inverse transform of the kernel, $c(\mathbf{x})$.

The discrete implementation of Eq. [1] is

$$M_c(\mathbf{k}) = \frac{1}{\phi(\mathbf{k})} \sum_{p,q,r \in \mathcal{T}} \frac{M_s(p, q, r)}{\hat{\rho}(p, q, r)} C(p - k_x, q - k_y, r - k_z) \quad [5]$$

where $\mathcal{T}$ is the set of k-space positions for the nonuniform samples, and $\mathbf{k}$ is now the discrete position of the Cartesian grid. Since in the discrete case the trajectory is defined as a collection of points, the density used in Eq. [1] must be an estimate $\hat{\rho}(i, j, k)$ of the density $\rho(i, j, k)$. Since the estimate $\hat{\rho}$ is not exact, an additional correction factor $\phi(\mathbf{k})$ is incorporated, computed as,

$$\phi(\mathbf{k}) = \sum_{p,q,r \in \mathcal{T}} \frac{1}{\hat{\rho}(p, q, r)} C(p - k_x, q - k_y, r - k_z)$$

that assures uniform weighting for the energy of M_c.

RESULTS

We employed the spherical stack of spirals and the density compensated cones trajectories in two experiments. The spherical stack of spirals presents the shortest imaging time as shown in Table 1 and can also easily be modified for anisotropic field of views. The cones trajectory is the fastest of the trajectories that do not need preparation time and possesses good flow properties in all directions.

These sequences were implemented on a commercial GE SIGNA 1.5T imager with the following restrictions for the gradients: $|G| \leq 1$ G/cm and $|dG/dt| \leq 2$ G/cm/ms.

Figure 12 shows three orthogonal slices taken from a 3D data set of the head using the spherical stack of spirals trajectory. The following parameters were used: field of view of 30 × 30 × 7.5 cm; resolution of 200 × 200 × 50 pixels (1.5 × 1.5 × 1.5 mm); tip angle of 30°; and a readout duration of 14.336 ms. The acquisition was done with 928 excitations at a TR of 60 ms (55.7 s). A simple windowed sinc excitation was used to select a slab of approximately 6.5 cm. The readout was done immediately following the refocusing lobe of the excitation.

A four dimensional (4D) acquisition was implemented employing the density compensated cones trajectory. The 4D data set is composed of a time series of 3D images. It was used to image the heart with a surface coil.

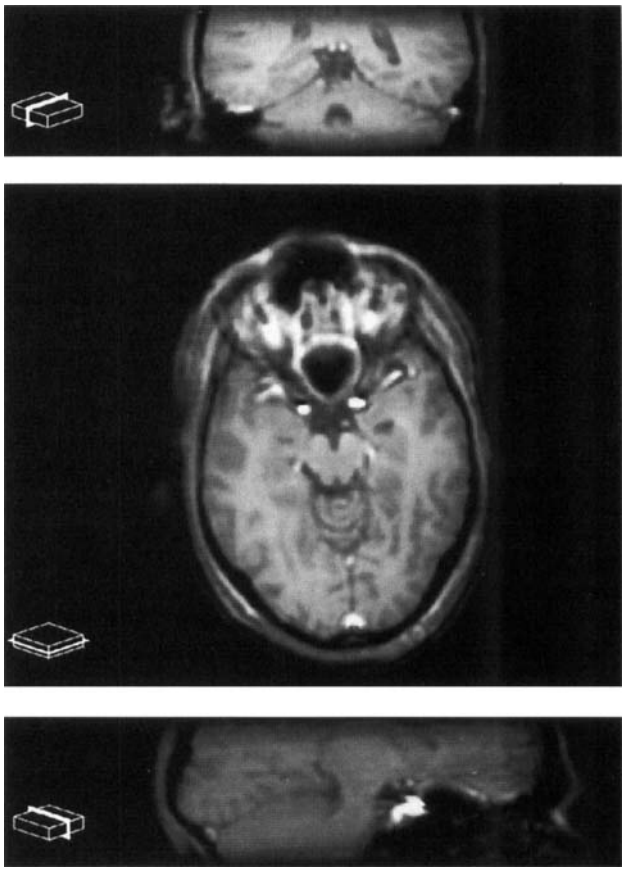

FIG. 12. Coronal, axial and sagittal slices of a 3D data set of the head acquired with a spherical stack of spiral in 55.7 s.

Lipids were not excited by the use of a spatially and spectrally selective excitation (19). The following parameters were used: spatial field of view of 20 × 20 × 20 cm; resolution of 100 × 100 × 100 pixels and 16 time frames (2 × 2 × 2 mm × 50 ms); excitation tip angle 30°; and a readout duration of 14.336 ms. Each 3D image requires 800 excitations, therefore the whole movie is acquired in 800 heart beats (retrospective gating was not employed).

Figures 13–15 show three slices in the three orthogonal planes of a 3D frame from a healthy volunteer. The movie was acquired in approximately 10 min with the subject lying prone and breathing normally. The images demonstrate the coronary vessels. The 3D acquisition allows the retrospective selection of any plane of view to maximize the potentially needed clinical information. While blood/muscle contrast is not large due to the sequence parameters other techniques may be used in conjunction to enhance the needed tissue contrast.

DISCUSSION

The choice of a 3D trajectory depends largely on the application. Some trajectories are better suited than others in terms of scan time, flow properties, TE and geometric considerations.

For applications in which the total scan time is important, the spherical stack of spirals requires the fewest number of excitations. Although it requires almost as

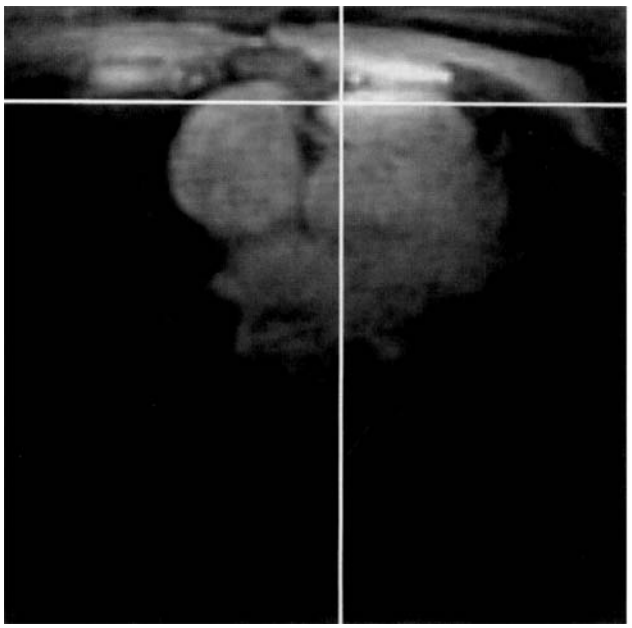

FIG. 13. Axial slice of a 3D data set of the heart acquired with a density compensated cones trajectory. Proximal right coronary artery is visible.

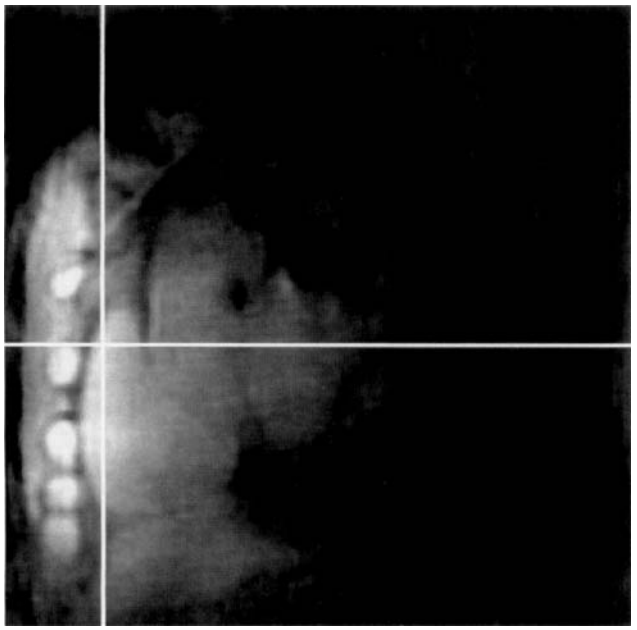

FIG. 14. Sagittal slice of a 3D data set of the heart acquired with a density compensated cones trajectory.

many excitations as the shells trajectory, it has the additional advantage that the reconstruction is more efficient, because it can be done as a set of 2D grids. For applications in which flow insensitivity is important, such as cardiac and angiographic applications, the density compensated cones trajectory is a good option. The demonstration of its good flow properties is beyond the scope of this paper. For anisotropic field of view or resolution, the spherical stack of spiral is appropriate because it makes it easy to add or subtract spirals in the direction perpendicular to their planes. Cones or shells are less amenable

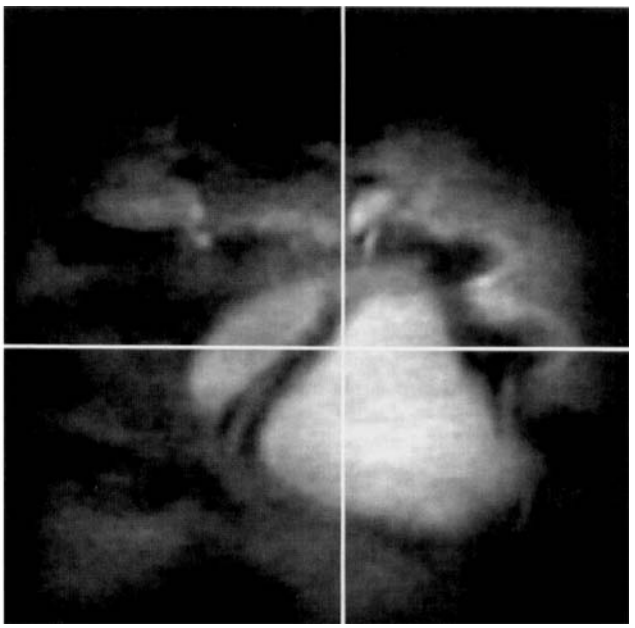

FIG. 15. Coronal slice of a 3D data set of the heart acquired with a density compensated cones trajectory. Distal portions of the right and left coronary arteries are visible.

to anisotropic field of view and resolution. For a fluoroscopy application in which different segments of k-space are updated at different rates (20), the shells trajectory is appropriate. It allows updating of the lower spatial frequency and the higher spatial frequency shells at different rates. For materials of short T_2, the trajectory should be any of the ones with no preparation time, such as cones, yarn, or spiral-PR.

When there is a triggering constraint such as with cardiac imaging or to obtain T_2 contrast with short TR, a RARE mode (more than one spin echo is used for readout) or a Turbo mode (small tip-angle excitations are used to acquire data during nonsteady state) are reasonable. The cones, yarn, and shells trajectories are well suited for these kind of implementations.

Angiography is an application where these 3D trajectories are appropriate. Preliminary time of flight and phase contrast angiograms has been obtained with the density compensated cones and spherical stack of spiral trajectories. Spectroscopic and functional imaging are other applications in which fast 3D imaging is desirable.

CONCLUSIONS

We designed and tested alternative k-space trajectories for faster 3D magnetic resonance imaging. The use of time-varying gradients and non-Cartesian sampling shortens the scan time by a factor of as much as 11 (compared with a conventional 3DFT), provides the flexibility for trading off SNR for scan time, and provides good insensitivity to flow and motion artifacts.

REFERENCES

1. K. Gluckert, B. Kladny, A. Blank-Schal, G. Hofmann, MRI of the knee joint with a 3-D gradient echo sequence. *Arch. Orthop. Traum. Surg.* **112**, 5–14 (1992).

2. M. Bomans, K. Hohne, G. Laub, A. Pommert, U. Tiede, Improvement of 3D acquisition and visualization in MRI. *Magn. Reson. Imaging* **9,** 597–609 (1991).
3. P. Brunner, R. R. Ernst, Sensitivity and performance time in NMR imaging. *J. Magn. Reson.* **33,** 83–106 (1979).
4. C. Meyer, B. Hu, D. Nishimura, A. Macovski, Fast spiral coronary artery imaging. *Magn. Reson. Med.* **28,** 202–213 (1992).
5. A. Macovski, Volumetric NMR imaging with time-varying gradients. *Magn. Reson. Med.* **2,** 29–40 (1985).
6. I. Shenberg, A. Macovski, Applications of time-varying gradients in existing magnetic resonance imaging systems. *Med. Phys.* **13,** 164–169 (1986).
7. A. Maudsley, G. Matson, J. Hugg, M. Weiner, Reduced phase encoding in spectroscopic imaging. *Magn. Reson. Med.* **31,** 645–651 (1994).
8. D. Nishimura, P. Irarrazabal, C. Meyer, A velocity *k*-space analysis of flow effects in echo-planar and spiral imaging. *Magn. Reson. Med.* **33,** 549–556 (1995).
9. J. O'Sullivan, A fast sinc function gridding algorithm for Fourier inversion in computer tomography. *IEEE Trans. Med. Imaging* **MI,** 200 (1985).
10. C. Meyer, A. Macovski, D. Nishimura, A comparison of fast spiral sequences for cardiac imaging and angiography, *in* "Proc., SMRM, 9th Annual Meeting, 1990," p. 403.
11. S. Wong, M. Roos, Strategy for sampling on a sphere with applications to 3D selective pulse design, *in* "Proc., SMRM, 12th Annual Meeting, 1993," p. 1178.
12. M. Lauzon, B. Rutt, Generalized *k*-space analysis and correction of motion effects in MR imaging. *Magn. Reson. Med.* **30,** 438–446 (1993).
13. P. Mansfield, Multi-planar image formation using NMR spin echoes. *J. Phys. C* **10,** L55–L58 (1977).
14. P. Mansfield, A. Howseman, R. Ordidge, Volumar imaging using NMR spin echoes: echo-volumar imaging (EVI) at 0.1 T. *J. Phys. E* **22,** 324–330 (1977).
15. D. Nishimura, J. Jackson, J. Pauly, On the nature and reduction of the displacement artifact in flow images. *Magn. Reson. Med.* **22,** 481–492 (1991).
16. G. Glover, J. Pauly, Projection reconstruction techniques for reduction of motion effects in MRI. *Magn. Reson. Med.* **28,** 275–289 (1992).
17. J. Jackson, C. Meyer, D. Nishimura, A. Macovski, Selection of a convolution function for Fourier inversion using gridding. *IEEE Trans. Med. Imaging* **10,** 473–478 (1991).
18. P. Irarrazabal, B. S. Hu, J. M. Pauly, D. G. Nishimura, Spatially resolved and localized real-time velocity distribution. *Magn. Reson. Med.* **30,** 207–212 (1993).
19. C. Meyer, J. Pauly, A. Macovski, D. Nishimura, Simultaneous spatial and spectral selective excitation. *Magn. Reson. Med.* **15,** 287–304 (1990).
20. C. Meyer, D. Spielman, A. Macovski, Spiral fluoroscopy, *in* "Proc., SMRM, 12th Annual Meeting, 1993," p. 475.